

Hybrid atomic orbital basis from first principles: Bottom-up mapping of self-energy correction to large covalent systems

Manoar Hossain, Joydev De, Joydeep Bhattacharjee
*National Institute of Science Education and Research,
HBNI, Jatni, Khurda, Bhubaneswar, 752050, Odisha, India*

Construction of hybrid atomic orbitals is proposed as the approximate common eigen states of finite first moment matrices. Their hybridization and orientation can be a-priori tuned as per their anticipated neighbourhood. Their Wannier function counterparts constructed from the Kohn-Sham(KS) single particle states constitute an orthonormal multi-orbital tight-binding(TB) basis resembling hybrid atomic-orbitals locked to their immediate atomic neighborhood, while spanning the subspace of KS states. The proposed basis thus not only renders predominantly single TB parameters from first-principles for each nearest neighbour bonds involving no more than two orbitals irrespective of their orientation, but also facilitate an easy route for transfer of such TB parameters across isostructural systems exclusively through mapping of neighbourhoods and projection of orbital charge centres. With hybridized $2s,2p$ and $3s,3p$ valence electrons, the spatial extent of self-energy correction(SEC) to TB parameters in the proposed basis are found to be localized mostly within the third nearest neighbourhood, thus allowing effective transfer of self-energy corrected TB parameters from smaller reference systems to much larger target systems, with nominal additional computational cost beyond that required for explicit computation of SEC in the reference systems. The proposed approach promises inexpensive estimation of quasi-particle structure of large covalent systems with workable accuracy.

A. Introduction

Setting a minimal TB basis for a given systems of atoms calls for appropriate orientation of orbitals at each atomic site in accordance with their immediate atomic neighbourhood, so that the nearest neighbour interactions can be represented by the least number of orbitals. In this direction, hybrid atomic orbitals have been used by quantum chemists since their introduction[1, 2] almost a century ago. Rational approaches for their construction[3–7] over the last several decades have been primarily focussed on partitioning systems into substructures which are spanned by groups of hybrid orbitals, leading to unambiguous partitioning of electrons into bonding orbitals and lone-pairs, and further into atomic orbitals. For such partitioning, notionally similar several approaches [4, 6, 8–11] have been proposed grossly based on the maximum overlap condition which in effect leads to localization of orbitals within the chosen subspace of molecular orbitals. In these approaches, either the overlap matrix[4, 6] or the first-order density matrices[10, 12], both of which are calculated typically in the basis of either the Slater type orbitals(STO)[13] or the Gaussian type orbitals(GTO)[14, 15], are generally transformed into block diagonal forms each spanned by orbitals centered on nearest neighbour atoms. The resultant hybrid orbitals involving atomic orbitals centred on more than one atoms[7, 16] render unambiguous bonding orbitals and bond-orders, while the ones like the *natural hybrid orbitals*(NHO)[12] or the *effective atomic orbital*(EAO)[11], which involve atomic orbitals of a single atom, describe the state of the orbitals of the atoms as they participate in bonds. Hybrid orbitals in the line of NHOs have been popularly constructed ab-initio at the HF level[17, 18].

A more explicit approach[19, 20] has been to construct the *generalized hybrid orbitals*(GHO) as combinations of STO with common Slater exponent and fixed position of nodes along bonds to assign their orientation. Expedient to clarify that in this paper we refer to bonds simply as the linear connectivity between atoms which are primarily nearest neighbours if not mentioned specifically. Much of these efforts were undertaken in aid to molecular mechanics calculation[21, 22] where the description of interactions between sub-structures eases with use of orbitals which are directed along bonds. Effective analytical models for such interactions have also been developed[23] recently for inexpensive deductive computation of properties of bulk as well as clusters of sp^x hybridized covalent systems. Notably unlike the GHOs, the NHOs or the EAOs by construction may not be oriented exactly along the bonds. In general for all such hybrid orbitals, their directed nature, maximal localization and orthonormality are not guaranteed simultaneously by construction. In a part of this work we explore simultaneity of these conditions in construction of hybrid atomic orbitals from first-principles proposed in this work.

Instead of overlap or density matrices, in this work we take recourse to the first moment matrices (FMM) due to their direct correspondence to localization. FMMs are known not to commute among each other in more than one dimension if projected on to a finite subspace of orthonormal states. We propose construction of hybrid atomic orbitals(HAO) as approximate eigen states of the FMMs within a finite subspace of Kohn-Sham (KS) states of isolated atoms. Orientation and hybridization of the proposed orbitals can be a-priori naturalized as per their anticipated neighbourhood. This substantially eases the effort of orientating them appropriately while transferring them from isolated atoms to the real sys-

tems, which eventually eases the interpretation of elements of the Hamiltonian. An orthonormal set of localized Wannier orbitals resembling the HAOs is further constructed in the basis of KS single particle states of the given system. These Wannier orbitals, which we refer in this paper as the *hybrid atomic Wannier orbitals* (HAWO), constitute a multi-orbital tight-binding (TB) basis locked to their immediate atomic neighbourhood by construction, and render hopping parameters involving effectively only two orbitals per bond. HAWOs thus offer easy transfer of the corresponding TB parameters to other iso-structural systems exclusively through mapping of neighbourhoods and projection of charge centres learned from HAOs. Effective transfer of TB parameters is demonstrated in nano-ribbons of graphene and hexagonal boron-nitride, C_{60} , and nano-diamonds and their silicon based counterparts. In particular, we show in the HAWO basis that it is possible to effectively transfer self-energy(SE) correction(SEC) of single particle levels from smaller reference systems to much larger iso-structural systems through TB parameters with minimal additional computational expense through the proposed mapping of multi-orbital TB parameters beyond the nearest neighbourhood.

I. METHODOLOGICAL DETAILS

A. Construction of hybrid orbitals

In a given direction, for example along \hat{x} , the most localized orbitals $\{\phi\}$ would diagonalize the corresponding FMM:

$$X_{ij} = \langle \phi_i | x | \phi_j \rangle. \quad (1)$$

This becomes clear by noting that the total spread of a finite set of N number of orbitals along \hat{x} is given by:

$$\Omega_x = \sum_{i=1, N} [\langle \phi_i | x^2 | \phi_i \rangle - |\langle \phi_i | x | \phi_i \rangle|^2], \quad (2)$$

which can be expressed as:

$$\begin{aligned} \Omega_x &= \sum_{i=1, N} \left(\sum_{j=1}^{\infty} X_{ij} X_{ji} - X_{ii} X_{ii} \right) \\ &= \sum_{i=1, N} \sum_{j \neq i} |X_{ij}|^2 \\ &= \sum_{i=1, N} \left(\sum_{j \neq i}^N |X_{ij}|^2 + \sum_{j=N+1}^{\infty} |X_{ij}|^2 \right). \end{aligned} \quad (3)$$

Diagonalization of X in the $N \times N$ subspace would therefore sets the first term in Eqn.(3) to zero, leading to minimization of total spread. Notably, X can be calculated directly as in Eqn.(1) only for isolated systems well separated from their periodic images. For periodic

system with non-zero crystal momentum, computation of X would essentially involve evaluation of geometric phases[24] of Bloch electrons evolved across the Brillouin Zone[25, 26]. Nevertheless, there exists therefore a unique set of orbitals which completely diagonalize X , and would also thereby have maximum localization along \hat{x} . Similar unique sets exist for \hat{y} and \hat{z} directions as well. However, the matrices X , Y and Z , when projected into a finite subspace of orthonormal states, do not commute with each other in general unless mandated by symmetries. This implies that a unique set of orbitals with maximum localization simultaneously in all three orthogonal directions would not exist in general. The same is true for Wannier functions (WF) in case of periodic systems with non-zero wave-vectors. Numerically localized Wannier functions [27, 28] therefore are not be unique and the choice of gauge used for their construction depends on the chosen criteria of localization.

We chose to look for the possibility to construct a set of localized orbitals which will be a reasonable compromise between the three unique sets of orbitals having maximum localization along the three orthogonal directions. We thus resorted to the condition of simultaneous approximate joint diagonalization [29] of the three FMMs: X , Y and Z . To compute such an approximate eigen subspace of the three FMMs, we adopted an iterative scheme based on generalization of the Jacobi method of matrix diagonalization[30], wherein, off-diagonal elements are iteratively minimized by applying rotation of coordinates by an optimally chosen angle. The extension of the method to more than one square matrices irrespective of whether they are commuting or not, is based on a proposed[29] choice of angle of rotation leading to complex rotation matrix U which has been proven[29] to minimize the composite objective function defined as :

$$\text{off}(UXU^\dagger) + \text{off}(UYU^\dagger) + \text{off}(UZU^\dagger) \quad (4)$$

where $\text{off}(A) = \sum_{1 \leq i \neq j \leq N} |A_{ij}|^2$ for an $N \times N$ matrix A . N being the number of orthonormal states used to compute X , Y and Z . U is a product of all the $N(N-1)/2$ complex plane rotations, one each for each pairs of (ij) for $i \neq j$. For a given (ij) the plane rotation $R(i, j)$ is an $N \times N$ identity matrix except for:

$$\begin{pmatrix} r_{ii} & r_{ij} \\ r_{ji} & r_{jj} \end{pmatrix} = \begin{pmatrix} c & \bar{s} \\ -s & \bar{c} \end{pmatrix} \quad (5)$$

where $c, s \in C$, $|c|^2 + |s|^2 = 1$.

It has been shown[29] that the objective function defined in Eqn.(4) is minimized if U is a product of $R(i, j)$ matrices as shown in Eqn.(5) whose elements are given as:

$$c = \sqrt{\frac{x+r}{2r}}; s = \frac{y-iz}{\sqrt{2r(x+r)}} \quad (6)$$

where

$$r = \sqrt{x^2 + y^2 + z^2}$$

and $[x, y, z]^\dagger$ being the eigen-vector corresponding to the highest eigen-value of a 3×3 matrix:

$$G(i, j) = \text{Real}(h^\dagger(X, i, j)h(X, i, j)) \\ + \text{Real}(h^\dagger(Y, i, j)h(Y, i, j)) \\ + \text{Real}(h^\dagger(Z, i, j)h(Z, i, j))$$

with:

$$h(A, i, j) = [a_{ii} - a_{jj}, a_{ij} + a_{ji}, i(a_{ji} - a_{ij})]. \quad (7)$$

Notably, given the form of $R(i, j)$, for a rotated matrix $A' = R(i, j)AR^\dagger(i, j)$ corresponding to plane rotation for the (ij) -th pair of elements of A , it is easily seen that $a'_{kk} = a_{kk}$ for $k \neq i$ and $k \neq j$, leading to the invariance:

$$\text{off}(A') + |a'_{ii}|^2 + |a'_{jj}|^2 = \text{off}(A) + |a_{ii}|^2 + |a_{jj}|^2.$$

owing to preservation of norm in similarity transformation. Therefore, minimizing $\text{off}(A')$ would naturally imply maximising $|a'_{ii}|^2 + |a'_{jj}|^2$, which further implies maximising $|a'_{ii} - a'_{jj}|^2$ since:

$$2(|a'_{ii}|^2 + |a'_{jj}|^2) = |a'_{ii} + a'_{jj}|^2 + |a'_{ii} - a'_{jj}|^2$$

and

$$a'_{ii} + a'_{jj} = a_{ii} + a_{jj}$$

owing to invariance of trace under similarity transformation. Therefore in our case the minimization of the objective function[Eqn.(4)] implies maximizing the separation between the charge centres of the i -th and the j -th orbitals, which is thus similar to the principle of the Foster and Boys[31] scheme of orbital localization. This becomes clear by rewriting the total spread [Eqn.(3)] for N orbital $\{\phi_i, i = 1, N\}$ as:

$$\Omega = \sum_{k=1,3} \sum_{i=1, N} \left(\sum_{j \neq i}^N |a_{ij}^k|^2 + \sum_{j=N+1}^{\infty} |a_{ij}^k|^2 \right) \quad (8)$$

where $A^{k=1,2,3} = X, Y, Z$. Eqn.(8) clearly suggests that minimization of the objective function in Eqn.(4) would minimize the first term in Eqn.(8), leading to minimization of the total spread. Eqn.8 also suggests that the total spread will reduce with increasing number of states (N) in the basis of which the first moment matrices are constructed.

We test the proposed approach first with FMMs computed in the basis of GTOs constructed for Ti with parameters from Ref.[32]. In Fig.1 we plot the charge centres ($\langle \phi | \vec{r} | \phi \rangle$) of the approximate eigen states of the first moment matrices. Evidently, the charge centres constitute coordination polyhedra around isolated atoms which are consistent in shape with those tabulated in Figs.6-8 in Ref.[33]. This agreement confirms the identity of the resultant orbitals as the hybrid orbitals and numerically establishes the connection between maximal localization and hybridization. Such a connection between

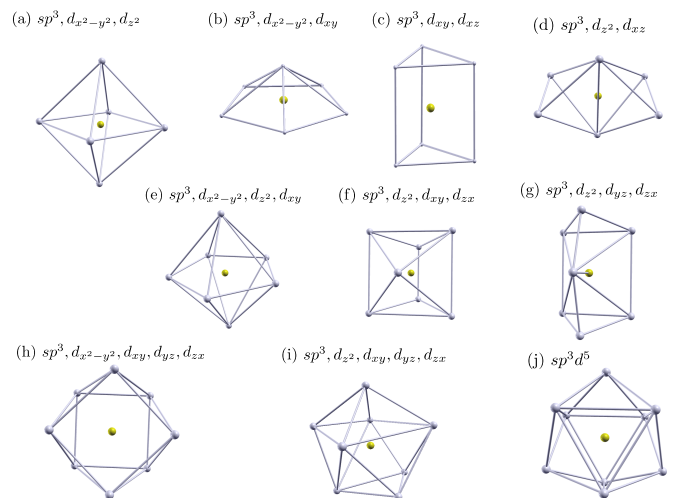


FIG. 1: Plots of charge centres (shown in gray) of the hybrid orbitals formed by the group of GTOs representing $3s, 3p$ and $3d$ orbitals of Ti (shown in yellow) constructed as per Ref.[32]

sp^3 hybridization and minimization of total quadratic spread of s and the three p orbitals has been analytically proven[34]. In this work however we do not use GTOs further and rather resort to KS states of isolated atoms. For example, for atoms of the p block, such as boron, carbon, nitrogen and silicon dealt with in this work, if the first moment matrices are constructed in the basis of three(four) KS states with lowest energies, namely, the one s like non-degenerate having the lowest energy and two (three) of the three p like degenerate states above the s like state, the approximate eigen subspace would render three(four) $2sp^2(2sp^3)$ hybridized orbitals. Notably, for isolated systems like molecules, clusters and nanostructures, the approximate common eigen spectrum of the FMMs computed within the manifold of occupied KS states results into partitioning[35–37] of the ground state charge density into bonding and localized orbitals.

1. Orientation and transfer of orbitals

Although as evident above that construction of HAOs for an isolated atom as such do not require any predefined directionality, the orientation of the HAOs asso-

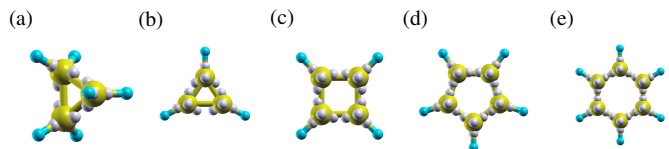


FIG. 2: Projected charge centres of HAOs are shown by gray spheres depicting their orientations around their host C atom shown in yellow.

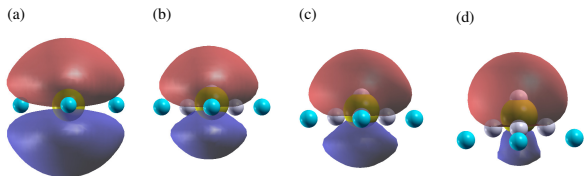


FIG. 3: (a-d): Evolution of a pure $2p_z$ orbital[(a)] from sp^2 hybridization background, to an sp^3 hybridized orbital due to increased deviation of the centres (cyan spheres) of the three confining potential spheres from co-planarity with the host atom (yellow sphere). Centres of HAOs are shown by gray spheres.

ciated with an atom can be nevertheless locked to their anticipated neighbourhood by placing the isolated atom within an external potential which represents the generic or exact atomic neighbourhood of the given atom in the actual system in which the HAOs are to be used. We construct such external potentials by placing weakly confining spheres with small constant negative potentials inside the spheres in place of exact or generic locations of neighbouring atoms as present in the actual system. For example, to lock sp^3 HAOs to a four coordinated tetrahedral neighbourhood, a tetrahedra of confining spheres is placed around the host C atom, leading to orientation of the sp^3 orbitals maximally in the direction of the confining spheres as seen in Fig.5(a). Typically we find confining potential amplitudes in the order of 0.01 eV and radius 0.5Å to be sufficient for the purpose. Such weak confinement in the vicinity causes change of KS energy eigen-values of isolated atoms in the order of 0.001 eV, and retains the shape of the lowest KS states which are used for construction of the HAOs, effectively unaltered. For sp^3 HAOs, the tetrahedra of the confining spheres can be an exact tetrahedra, as in case of bulk Si, or a strained tetrahedra, as in case of cyclopropane. As evident in Fig.2(a) for cyclopropane, and in Fig.2(b-e) for planar molecules C_nH_n , the projected charge center of the HAOs (shown in gray) symmetrically deviate away from the C-C bonds with decreasing C-C-C angle as we go from C_6H_6 to C_3H_3 . For all of these molecules the HAOs were constructed with the weakly confining spheres placed around the host C atom exactly as per their nearest neighbours in the molecules, resulting into HAOs largely retaining their pure sp^3 nature but oriented symmetrically about the directions of the confining spheres from the host atoms. The placement of confining potential spheres thus provide a gross directional reference for orientation of the full set of the HAOs.

Position of charge centres of the HAOs are learned in terms of the directions of the confining spheres from the isolated host atom. Such learnings are subsequently used in projecting centres of HAOs around the corresponding atom in a given system, as seen for the molecules in Fig.2, and nano-diamonds in Fig.4. While transferring HAOs from their nursery of isolated host atoms, to their matching host atoms in a given system, HAOs are rotated such

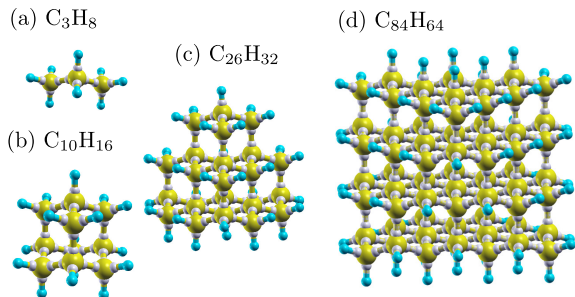


FIG. 4: C_nH_m systems with projected charge centre of HAOs shown as gray spheres, used in this work as example of sp^3 hybridized covalent systems.

that their actual charge centres align along the direction of their projected centers from the matching host atoms.

In addition to providing reference for orientation, the confining spheres can have an important role in deciding the level of hybridization of the HAOs. This becomes evident by noting that if we use four KS states and three confining sphere coplanar with the host atom, then instead of forming four sp^3 orbitals, the HAOs separate into three $2sp^2$ orbitals and one $2p_z$ orbital, as evident from the unhybridized shape of the $2p_z$ orbital in Fig.3(a). Fig.3(a-d) shows evolution of the $2p_z$ HAO from a pure orbital perpendicular to the plane of sp^2 hybridization, towards a $2sp^3$ hybridized orbital, with increasing non-coplanarity of the confining spheres with the host atom. HAOs with such intermediate hybridization ($2sp^{2+} + 2p_z^+$) has been used for C_{60} [Fig.8]. However, stronger confining potentials are found necessary to influence hybridization of KS states, typically in the order of 1eV for C atoms, such that the orbitals align along the confining spheres. The confining potentials in this case therefore does lead to minor modification of shape of the KS states, and thereby of the HAOs as well, although not quite obvious at the iso-surfaces plotted in Fig.3(a-d). However the values of TB parameters calculated in the basis of their Wannierized counterparts in C_{60} suggests that the overall shape of those orbitals are largely retained close to the sp^2 orbitals. Notably, we could have used stronger confinement to align the HAOs in C_3H_6 , C_3H_3 or C_4H_4 as well like we did for C_{60} , but the degree of confinement would have to be much high than that used for C_{60} , which would have substantially altered the shape of the HAOs themselves, since it is obvious that with pure s, p_x, p_y, p_z orbitals it is impossible to form any set of hybrid orbitals in which two orbitals can have relative orientation less than 90° .

B. Wannier functions based on HAOs

The next step is to construct orthonormalized Wannier functions from the KS states following the HAOs

transferred to a given system. The transferred HAOs constitute a non-orthogonal basis of hybridized atomic orbitals. In the general framework of periodic systems with non-zero wave-vectors (\vec{k}) we begin with constructing a non-orthogonal set of quasi-Bloch states as:

$$\tilde{\psi}_{\vec{k},j}(\vec{r}) = \frac{1}{\sqrt{N}} \sum_{\vec{R}} e^{i\vec{k}\cdot\vec{R}} \phi_{\vec{R},j}(\vec{r}), \quad (9)$$

where $\phi_{\vec{R},j}(\vec{r})$ is the j -th HAO localized in the unit-cell denoted by the lattice vector \vec{R} spanning over N unit-cells defining the Born-von Karman periodicity. The projections of the non-orthogonal quasi-Bloch states on the orthonormal Bloch states constructed from the KS single-particle states at all allowed \vec{k} , are calculated as:

$$O_{\vec{k},m,j} = \langle \psi_{\vec{k},m}^{KS} | \tilde{\psi}_{\vec{k},j} \rangle. \quad (10)$$

Elements of O thus record the representation of the HAOs within the manifold of KS bands considered. Overlaps between the non-orthogonal quasi-Bloch states within the manifold of the considered KS states are therefore calculated as:

$$S_{\vec{k},m,n} = \sum_l O_{\vec{k},l,m}^* O_{\vec{k},l,n}. \quad (11)$$

The degree of representability of HAO ϕ_n , within the set of KS states considered, is guaranteed by setting a lower cutoff on individual $S_{\vec{k},n,n}$ values to be typically more than 0.85. For all the system studied in this work, the above criteria is found to be satisfied by the lower bound on the number KS states, which is set by the total number of valence orbitals of all atoms of a given system. A new set of orthonormal Bloch states from the KS single particle states are subsequently constructed using the Löwdin symmetric orthogonalization [38] scheme as:

$$\Psi_{\vec{k},n}(\vec{r}) = \sum_m S_{\vec{k},m,n}^{-\frac{1}{2}} \sum_l O_{\vec{k},l,m} \psi_{\vec{k},l}^{KS}(\vec{r}), \quad (12)$$

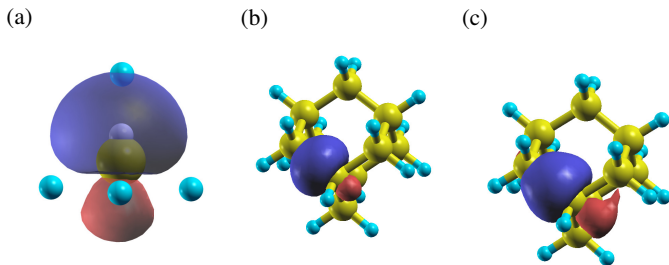


FIG. 5: (a): HAO representing a sp^3 orbital of an isolated C atom (yellow sphere) used in this work. Charge centre of the orbital is shown in gray. Centres of the confining spheres used to determine gross orientation are shown in cyan. (b): HAO shown in (a) transferred to a C atom in an adamantane ($C_{10}H_{16}$) molecule, (c): the corresponding HAWO.

where the sum over l spans the KS states considered and the sum over m takes care of the orthonormalization. Subsequently, a localized set of orthonormal Wannier functions are constructed as:

$$\Phi_{\vec{R}',j}(\vec{r}) = \frac{1}{\sqrt{N}} \sum_{\vec{k}} e^{-i\vec{k}\cdot\vec{R}'} \Psi_{\vec{k},j}(\vec{r}). \quad (13)$$

In this process the Löwdin symmetric orthogonalization clearly provides a choice of gauge for linear combination of KS states such that the resultant Wannier functions $\{\Phi_{\vec{R}',j}(\vec{r})\}$ resemble the corresponding HAOs $\{\phi_{\vec{R},j}(\vec{r})\}$ as much possible within the manifold of KS states considered. Hence we refer to these Wannier functions as the hybrid atomic Wannier orbitals (“HAWO”). In Fig.5 we show an HAO before and after transfer to adamantane and the corresponding HAWO constructed from the KS states of adamantane. HAWOs can thus be considered as analogue of NHOs constructed from a given set of KS states with acceptable representability.

1. TB parameters in HAWO basis

TB parameters in the HAWO basis are computed from energetics of KS single particle states as:

$$t_{\vec{R}',\vec{R},i,j} = \langle \Phi_{\vec{R}',i} | H^{KS} | \Phi_{\vec{R},j} \rangle = \sum_{\vec{k}} e^{i\vec{k}\cdot(\vec{R}'-\vec{R})} \sum_l (OS^{-\frac{1}{2}})_{li}^* (OS^{-\frac{1}{2}})_{lj} E_{\vec{k},l}^{KS} \quad (14)$$

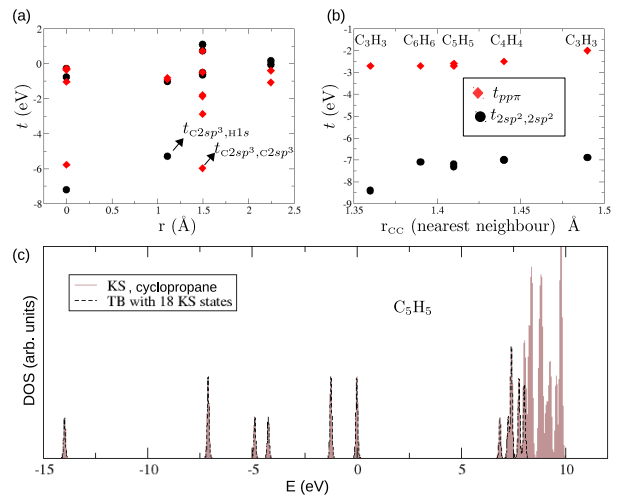


FIG. 6: (a): TB parameter calculated for cyclopropane; (b): Nearest neighbour TB parameters between in-plane and out of plane orbitals in C_3H_3 , C_4H_4 , C_5H_5 and C_6H_6 molecules (shown in Fig.2) arranged as a function of C-C bond lengths available in the molecules. (c) DOS calculated from 50 lowest KS eigen-values, compared with DOS from eigen-values of TB hamiltonian constructed from 18 lowest KS states, 18 being the total number of valence orbitals of cyclopropane.

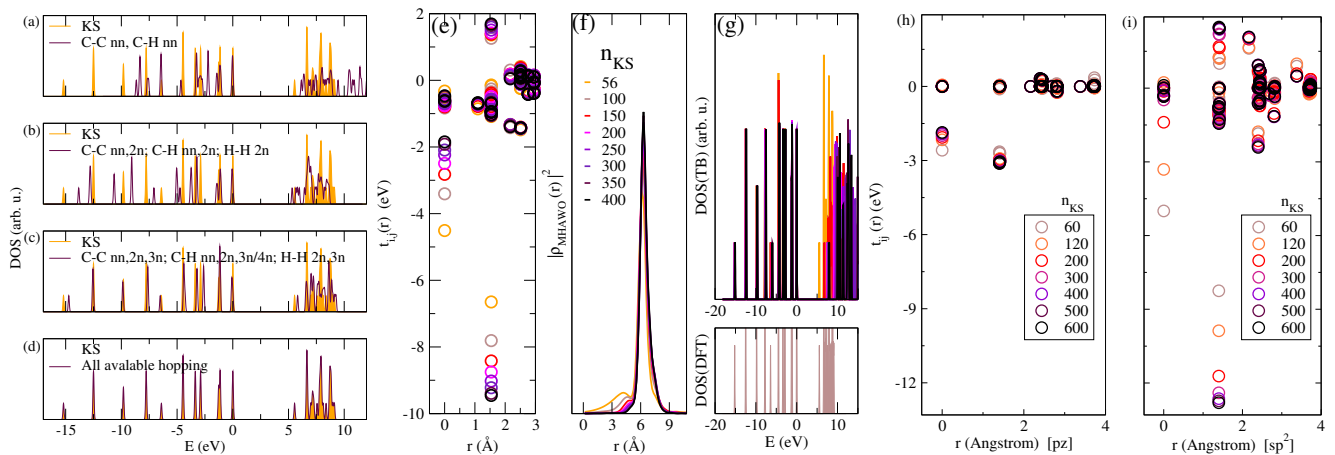


FIG. 7: For $C_{10}H_{16}$, (a-d): Evolution of density of states(DOS) with increase in range of hopping starting from (a): the nearest neighbour (nn) to (d): all available hopping graduating through hopping between second (2n) and third (3n) nearest neighbours and beyond. Convergence of (e): TB parameters and (f): spatial localization of $2sp^3$ orbitals, and (g): TB DOS, in terms of the number of KS states used in construction of HAWOs as mentioned in the legend of (f). KS DOS is shown below (g). Similar convergence of TB parameters for (h): $2p_z$ and (i): $2sp^2$ orbitals in AGNR ($3p+1$, $p=2$).

Notably, similar TB parameters have been derived in the last two decade from first principles based on the either the maximally localized Wannier function [39–44] or atomic orbitals [45, 46] constructed from KS states. Much effort has been reported in deriving TB parameters through projection of KS states on pseudo-atomic orbitals [47, 48] as well. However, attempts to calculate TB parameters in hybrid atomic orbital basis constructed from first-principles, as proposed in this work, has been limited so far primarily to analytical models[49, 50].

In Fig.6(a) for cyclopropane, we plot the TB parameters calculated as per Eqn.(14) for two HAOs participating dominantly in a C-C bond and a C-H bond. The t_{sp^3, sp^3} is comparable to the that in adamantane ($C_{10}H_{16}$)[Fig.12] despite the substantial misalignment[Fig.2] of HAO and the C-C bond in cyclopropane while perfect alignment of the two in $C_{10}H_{16}$. The hopping parameters are obtained with 18 KS states which is same as the total number of valence orbitals of all the atoms, resulting thereby into density of states in exact agreement with that obtained from DFT [Fig.6(c)] as discussed above in the next paragraph. In Fig. 6(b) we plot hopping parameters for π and σ bonds as a function of C-C bond lengths available in planar C_3H_3 to C_6H_6 molecules. As evident in Fig.2, the best alignment of the HAOs along the C-C bond is possible for C_6H_6 and the worst is obviously for the shorter bond of C_3H_3 and similarly for C_3H_6 . Yet, the highest in-plane hopping parameter in terms of magnitude is found for the shorter bond of C_3H_3 , which is about 20 % more than that of the C-C in-plane bond of benzene, whereas the C-C bond length in benzene only about 2.2 % more than the shorter bond of C_3H_3 . Similarly, the C-C nearest neighbour hopping parameter as well as the bond length in C_3H_8 , both are within 1 % of those of C_3H_6 , whereas in C_3H_8 the HAOs are almost perfectly aligned along the

C-C bond [Fig.4] while in C_3H_6 they are misaligned by more than 20° . These results can possibly be explained by the inherent bent nature the bonds[51] in C_3H_6 and C_3H_3 , reflected by the symmetric misalignment of the HAOs along the two C-C bonds while maintaining perfect alignment along the C-H bonds. We plan to examine this aspect for bent bonds in details in future.

As evident in Fig.7(a) for $C_{10}H_{16}$ the edge of the valence band is already well described if we consider only the nearest neighbour hopping in the HAWO basis. However, as shown in Fig.7(b) onwards, the match of DOS from TB and DFT improves drastically with increasing extent of hopping considered up to the second nearest neighbour. This is immediately understood by noting the non-nominal positive valued of the second nearest hopping element plotted in figure Fig.7(e), arising due to proximity of lobes of different signs of the two HAOs. In Fig.7(e-g), we demonstrate evolution of the TB parameters, HAWOs, and DOS from TB, as function of number of KS states considered for construction of HAWOs. The rationale for this analysis is the possibility that the anti-bonding subspace may not be adequately represented by the unoccupied KS states if we restrict the total number of KS states to be same as the total number of HAOs associated with all the atoms, which is same as the total number of valence orbitals of all the atoms. Indeed we see clear convergence of shape of HAWO [Fig.7(f)] as well as the corresponding TB parameters[Fig.7(e)] if we consider KS states in excess of the total number of HAOs. Fig.7(h,i) suggests that the convergence can be much quicker for un-hybridized orbitals like $2p_z$, compared to hybridized orbitals like sp^2 and sp^3 , since the un-hybridized orbitals primarily constitutes the edges of the valence and conduction bands. However, the TB DOS expectedly starts deviating from the DFT DOS more in the conduction band [Fig.7(g)]

if we include more KS states beyond the total number of HAOs, owing to the semi-unitary nature of the net transformation matrix ($OS^{\frac{1}{2}}$) implied in Eqn.(12) which will be rectangular in such scenarios. It is thus important to decide on the number of KS states to be considered depending on the purpose. If the aim is to represent only the valence bands through well localized HAWOs, then it may be prudent to look for convergence of HAWOs in terms of KS states. But if band-gap needs to be represented accurately by the TB parameters then the number of KS states should be kept same as the total number of valence orbitals.

C. Bottom-up mapping of TB parameters

The HAWO basis derived from the KS states offer a multi-orbital TB basis which are by construction locked to the local coordination as per the atomic neighbourhood of each atom. The TB parameters derive in such a basis should therefore be transferable from one system to another with matching atomic environment. A key aim of this work is to demonstrate such transferability for effective transfer of multi-orbital TB parameters in the HAWO basis from smaller reference systems to larger target systems. The mapping of TB parameters is done in two steps.

(1) Pairs of atoms of the target system, (not limited to nearest neighbours, are mapped on to pairs of atoms in the reference system based on a collection of criteria.

(2) Among the mapped pair of atoms, pair of system orbitals are mapped to pair of reference orbitals through mapping of their respective projected charge centres. In step (1) the criteria to map pairs of atoms include matching structural parameters such as their spatial separation and their individual nearest neighbourhoods characterised in terms of the type of neighbouring atoms and angles made by nearest neighbours on the atoms. In particular, we use a parameter calculated as:

$$\zeta_i = \sum_j^{N_i} Z_j w(r_{i,j}) \quad (15)$$

where N_i is the number of neighbours of the i -th atom within a suitably chosen cutoff radius, w being a weight factor which is a function of the distance $r_{i,j}$ of the j -th neighbour of the i -th atom, and Z_i a characteristic number to be associated with each type of atom. Z_i can be chosen to be the atomic weight, as we mostly used in this work, or a similar number which can facilitate identification of a type of neighbourhood or a region of the system through values of ζ . In this work we chose the weight factor w to be 1.0 within half of the cutoff radius beyond which the factor is smoothly reduced to zero using a cosine function. The choice of cutoff radius depends on the size of the reference system. It should neither be too large for variations to average out, nor should it be too small to become insensitive to morphological variations

in the reference system itself. ζ allows us to map atom pairs effectively through prudent choice of values of $\{Z_i\}$ since it would allow assessment of proximity of atoms to edges, interfaces or any kind of structural inhomogeneity without any exhaustive structural relaxation.

In step 1, the minimum of the deviation:

$$|\zeta_1^{\text{target}} - \zeta_1^{\text{reference}}| + |\zeta_2^{\text{target}} - \zeta_2^{\text{reference}}|$$

obtained within a range of allowed deviation of structural parameters, is used as the criteria to choose matching pairs of atoms between target and reference systems.

Like in step 1, in step 2 as well, the mapping of one or a pair of HAOs from the reference to target systems is done based on matching structural parameters, as well as a parameter calculated as:

$$\xi_i = \sum_j^{N_i} \zeta_j w^{WC}(r_{i,j}) \quad (16)$$

where ζ_j corresponds of the j -th atom in the neighbourhood defined by w^{WC} around of the projected charge centre of the i -th HAO. Angle made by the directions of the projected charge centres of the HAOs from their respective host atoms is a key matching parameter in step 2. Additionally, if the HAOs belong to different atoms then the dihedral angle made by the centres of the HAOs through the axis connecting their host atoms, is also a key parameter. Thus in step 2, the minimum of the deviation

$$|\zeta_1^{\text{target}} - \zeta_1^{\text{reference}}| + |\zeta_2^{\text{target}} - \zeta_2^{\text{reference}}|$$

within acceptable deviations of structural parameters, defines matching pairs of HAOs.

As an example we show mapping from a small curved finite patch[Fig.8(a)] to C_{60} . Since C_{60} constitutes a curved surface without any edge, mapping should be done from the inner most neighbourhood of the chunk. Since in C_{60} , the angles made by nearest neighbours at a given atom differ distinctly depending on whether an angle opens inside a pentagon or a hexagon, the matching parameters for mapping are mostly structural, primarily the direct and dihedral angles. The reference patch is cropped from C_{60} and passivated by H. We fix ζ tolerance to zero which implies that C_{60} is getting mapped from only six C atoms of the patch [Fig.8(a)] having all C neighbours. Given the curvature of C_{60} , we chose to use confining spheres to influence the hybridization of sp^2 HAOs in order to break their coplanarity and align them along nearest neighbour C-C bonds, as shown in Fig.3(c) where the placement of confining potential spheres are as per the nearest neighbourhood in C_{60} . The projected charge centres of HAOs with intermediate hybridization ($2sp^{2+} + 2p_z^+$) between ($sp^2 + p_z$) and sp^3 shown in Fig.8(c), is used to map from that of the reference shown in Fig.8(b). TB parameters $t_{2sp^{2+}, 2sp^{2+}}$ for the shorter and longer C-C bonds are about -6.9 eV and

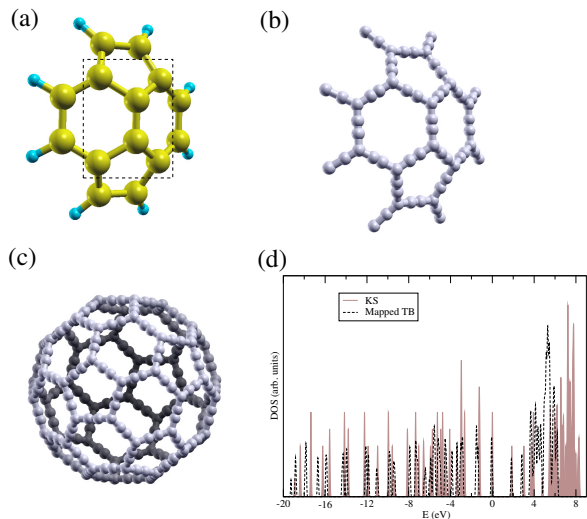


FIG. 8: (a): Structure of reference system, and (b): the corresponding charge centres of HAOs with intermediate hybridization ($2sp^2 + 2p_z^+$) between sp^2 and sp^3 . (c): Projected charge centre with similar hybridization for C_{60} . (d): Corresponding matches of DFT DOS with TB DOS with parameters mapped from the reference system.

-6.5 eV, whereas $t_{2p_z^+, 2p_z^+}$ are about -2.36 eV and -2.0eV. The match of the DFT DOS with the DOS from TB parameters mapped from the reference system is shown in Fig.8(d), which can be further improved beyond the valence band by considering HAOs for excited states, which will be taken up in a subsequent work on optical properties.

D. Self-energy correction of TB parameters

Self-energy corrected TB parameters $\{t_{\vec{R}', \vec{R}, i, j}^{QP}\}$ in the HAWO basis are calculated by substituting $E_{k,n}^{KS}$ in Eqn.(14) by quasiparticle energies $E_{k,n}^{QP}$ obtained at the G_0W_0 level which is the first order non-self-consistent GW approximation of MBPT[52] [53]. Within the GW approximation, the quasi-particle energies are approximated as:

$$E_{k,n}^{QP} = E_{k,n}^{KS} + \langle \psi_{k,n}^{KS} | \Sigma - V_{xc}^{KS} | \psi_{k,n}^{KS} \rangle, \quad (17)$$

where V_{xc}^{KS} is the mean-field exchange-correlation potential and Σ [54] is the self-energy operator derived by considering the many-electron effects as perturbation treated within a self-consistent framework of Dyson's equation formulated in terms of the one-particle dynamic non-local Green's function constructed from the KS states. Similar efforts have been reported in recent years on incorporating SEC in TB parameters computed in terms of the MLWFs[55–57]. Incorporation of SEC in TB parameters has also been attempted through matching specific bands of the QP structure[58–60].

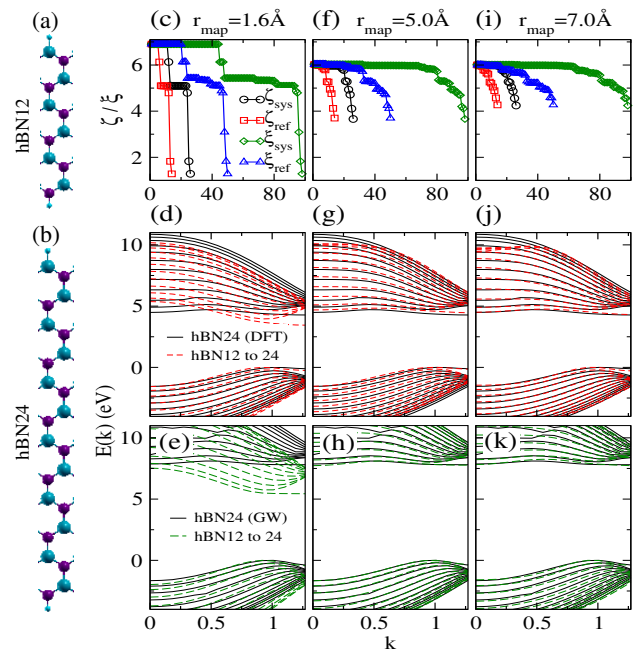


FIG. 9: (a,b) Hexagonal zigzag boron nitride nanoribbons(hZBNR: hBN), hBN12 and hBN24 respectively. (c,f,i) Plot of ζ and ξ values “ref”(reference hBN12) and “sys”(target hBN24) for different spatial ranges of neighbourhood considered for mapping. (d,g,j) Matching of DFT band-structure and mapped TB band-structure for increasing r_{map} . (e,h,k) Matching of DFT+ G_0W_0 band-structure and mapped self-energy corrected TB band-structure for increasing r_{map} .

II. COMPUTATIONAL DETAILS

Electronic structures of the ground states of all the systems considered in this work are calculated using the Quantum Espresso (QE) code[61] which is a plane wave based implementation of DFT. We have used norm conserving pseudo-potentials with the Perdew-Zunger (LDA) exchange-correlation[62] functional and a plane wave cutoff of 60 Rydberg for wave-functions and commensurately more for charge density and potential. Variable cell structural relaxation has been carried out for all periodic systems. We used a $1 \times 1 \times 15$ Monkhorst-Pack grid of k-point for AGNRs and $1 \times 1 \times 29$ for ZGNRs as well as for ZBNNRs. Self-energy correction to single particle levels have been estimated at the non-self-consistent G_0W_0 level of GW approximation implemented in the BerkeleyGW code[63]. To calculate the static dielectric matrix required for computation of the self-energy operator, the generalized plasmon-pole model[54] is used to extend the static dielectric matrix in the finite frequencies. For all the nanoribbons parameters are chosen from Ref.[64]. In house implementation interfaced with the QE code is used for generation of HAOs, HAWOs from KS states, calculation of TB parameters in the HAWO basis, and mapping of TB parameters from reference to target systems.

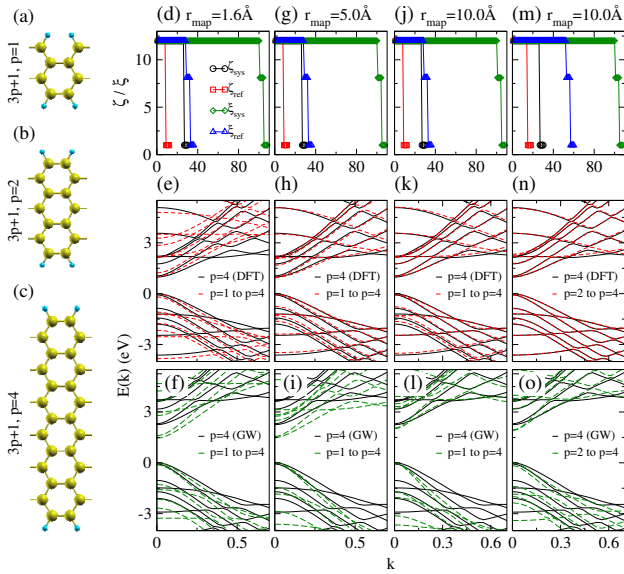


FIG. 10: (a,b,c) Armchair graphene nanoribbons (AGNR) of family $n=3p+1$ with $p=1$, $p=2$ and $p=4$ respectively. (d,g,j,m) Plot of ζ and ξ values “ref”(reference $p=1$ (in d,g,j) and $p=2$ (in m)) and “sys”(target $p=4$) for different spatial ranges (r_{map}) of neighbourhood considered for mapping. (e,h,k,n) Matching of DFT band-structure and mapped TB band-structure for increasing r_{map} . (f,i,l,o) Matching of DFT+ G_0W_0 band-structure and mapped self-energy corrected TB band-structure for increasing r_{map} .

A. Mapping self-energy corrected TB parameters in HAWO basis

1. Nanoribbons

We have recently reported[65] estimation of quasi-particle(QP) band-gap for graphene and hBN nanoribbons based on SE correction to TB parameters mapped from narrower ribbons in the basis of a single $2p_z$ electron per atom. The transfer was made explicitly by identifying equivalent atoms based on proximity to the ribbon edges as shown in Fig.2(c-e), Fig.3(f) and Fig.5(a) in Ref[65]. In this section we begin by systematizing the process of identifying the equivalent atoms through the mapping mechanism proposed in Sec.IC. The identification is primarily based on ζ values for atoms and ξ values for HAO charge centres wherever sufficient variations of ζ and ξ are available in the reference systems, as demonstrated in Fig.9(c,f,i) and Fig.11(c,f,i) for hBN and ZGNR respectively. Whereas, mapping of AGNR from $p=1$ to $p=4$, as shown in Fig.10(d,g,j,m), calls for matching of structural parameters as the key strategy for mapping, since the width of reference AGNR with $p=1$ of the $3p+1$ family, is narrow enough and have only two types of C atoms per unit-cell.

For hBN, acceptable match[Fig.9(g,j and h,k)] between explicitly computed band-structure, and the same computed from TB parameters with only $2p_z$ orbitals

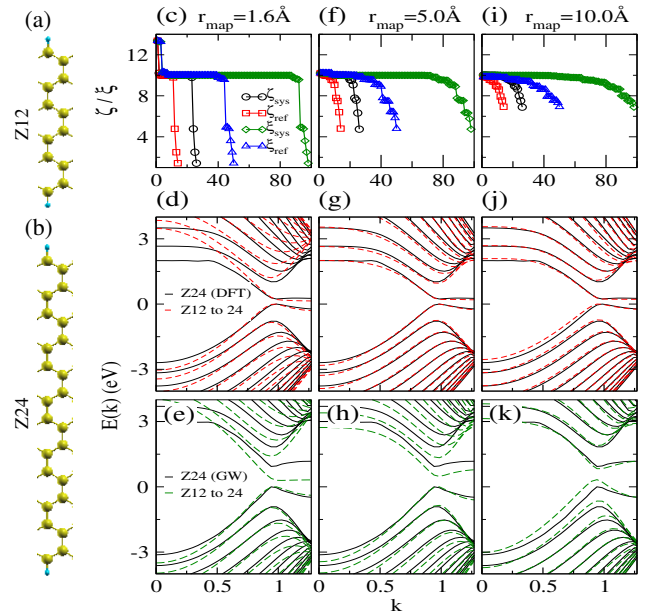


FIG. 11: (a,b) Zigzag graphene nanoribbons (ZGNR: Z, Z12 and Z24 respectively). (c,f,i) Plot of ζ and ξ values “ref”(reference Z12) and “sys”(target Z24) for different spatial ranges of neighbourhood considered for mapping. (d,g,j) Matching of DFT band-structure and mapped TB band-structure for increasing r_{map} . (e,h,k) Matching of DFT+ G_0W_0 band-structure and mapped self-energy corrected TB band-structure for increasing r_{map} .

mapped from a narrower ribbon [Fig.9(a)], is achieved simultaneously at the DFT and DFT+ G_0W_0 levels, with hopping considered within the range no less than 5\AA . Whereas a higher spatial range of mapping of self-energy corrected TB parameters is required for matching of band-structure at the DFT+ G_0W_0 level for AGNR

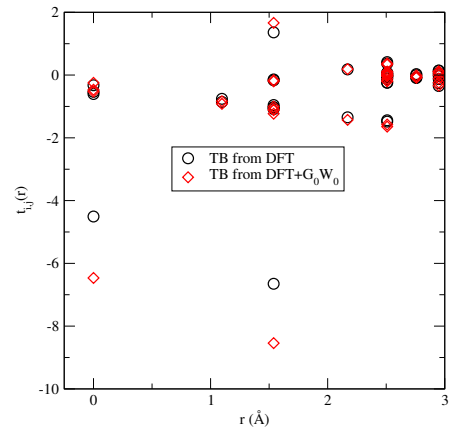


FIG. 12: TB parameters involving a C atom in $C_{10}H_{16}$ with three C neighbours, computed using 56 KS states with and without SEC at the G_0W_0 level, and plotted as a function of distance from the atom. TB parameters from DFT are same as those plotted in Fig.7(e).

[Fig.10(l)], and more so for ZGNRs [Fig.11(k)] with smaller band-gaps. Notable for AGNR, the match of self-energy corrected band edges for $p=4$ naturally improve with mapping from $p=2$ [Fig.10(o)]. These trends simply relate to the degree of localization of the states at the band edges - the more they are delocalized the larger is the spatial range within which the self-energy correction to TB parameters are to be considered.

2. Nano-diamonds

Fig.12 suggests that the extent of SEC to TB parameters are spatially limited mostly within the third nearest neighbourhood, implying possible transferability of SE corrected TB parameters to large covalent systems from smaller reference systems of which are large enough to accommodate the full spatial range of non-nominal SEC to TB parameters. Accordingly, mapping in nano-diamonds is demonstrated with C_3H_8 and $C_{10}H_{16}$ (adamantane) as reference systems to map to nano-diamonds $C_{26}H_{32}$ (pentamantane) and $C_{84}H_{64}$.

We start with attempts to map $C_{10}H_{16}$, $C_{26}H_{32}$ and $C_{84}H_{64}$ targets from C_3H_8 reference in sp^3 HAO basis. The mapping process starts with plotting the distance of atom pairs (C-H, C-C, H-H) for target and reference systems. As seen in Fig.13(a) there is one-to-one correspondence of C-C bonds between C_3H_8 and all targets up to approximately 2.5\AA , which is the second nearest C-C distance. For C-H and H-H pairs, such correspondence exists up to about 3\AA and 3.75\AA respectively. These correspondences decide the range of hopping parameters to be mapped. Notably, C_3H_8 has two varieties of C atoms - one with two(two) C(H) neighbours, and the other with one(three) C(H) nearest neighbours, whereas, $C_{10}H_{16}$ has C atoms with three(one)

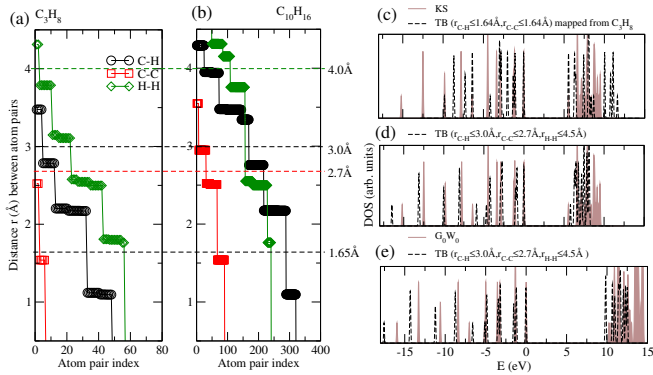


FIG. 13: Distribution of distance between pairs of atoms in (a): reference (C_3H_8) and (b): target ($C_{10}H_{16}$) systems. (c-d) Match between DFT DOS and mapped TB DOS as demonstrated of efficacy of mapping of TB parameters from C_3H_8 to $C_{10}H_{16}$ with increasing spatial range of neighbourhood considered for mapping. (e) Match between DFT+ G_0W_0 DOS and mapped self-energy corrected TB DOS.

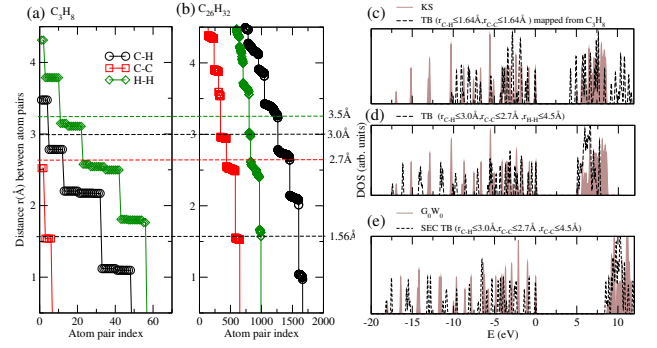


FIG. 14: Distribution of distance between pairs of atoms in (a): reference (C_3H_8) and (b): target ($C_{26}H_{32}$) systems. (c-d): Match between DFT DOS and mapped TB DOS as with an increasing spatial range of neighbourhood considered for mapping. (e): Match between DFT+ G_0W_0 DOS and mapped self-energy corrected TB DOS.

C(H) neighbours and two(two) C(H) neighbours. Additionally, $C_{26}H_{32}$ and $C_{84}H_{64}$ have C atoms with all C nearest neighbours(nn). Exact match of ζ between all atoms of reference and target systems is thus impossible in these examples. Matching ζ and ξ will therefore be less effective in mapping from C_3H_8 . Also, since there is only one C atom with two(two) C(H) neighbours in C_3H_8 , matching ζ can be restrictive in terms the variety of orientations. We thus opt for matching structural parameters within a tolerance for ζ set to the minimum difference of ζ values between similar type of atoms in reference and target systems to ensure maximal matching of ζ besides finer matching of structural parameters. As obvious, a better choice of reference system than C_3H_8 with C atoms having all varieties of neighbourhood can be easily made. However, we deliberately chose to test mapping from C_3H_8 which is the smallest possible reference system with just one C atom with two(two) C(H) neighbours, since such C atoms dominates the surfaces of the nano diamonds and are thereby expected to host the states at the edges of the valence and conduction bands. Surprisingly, as evident in Fig.13(c), with mapping of only the nn-hopping terms from C_3H_8 to $C_{10}H_{16}$, the mapped TB DOS already matches reasonable well with DFT DOS of $C_{10}H_{16}$ in terms of the band-gap and DOS around band edges. With increase in range of hopping to 2.7\AA (nn,2n), 3\AA (nn,2n,3n) and 4\AA (2n,3n,4n) for C-C, C-H and H-H pairs based on availability of one-to-one mapping[Fig.13(a,b)] the match of mapped TB DOS and DFT DOS[Fig.13(d)] extends deeper into the valence band. The quality of match improves further with additional mapping of C-H and H-H atom pairs up to 4.5\AA [Fig.13(e)] without compromising on tolerance factors. Notably, the range of hopping of C-H and H-H, although are more than that of C-C, are actually consistent with the range of C-C hopping, since the farthest H atoms considered are associated with two second nearest C atoms. The same mapping parameters are then used to map self-energy corrected TB (SEC-TB) parameters of C_3H_8 to

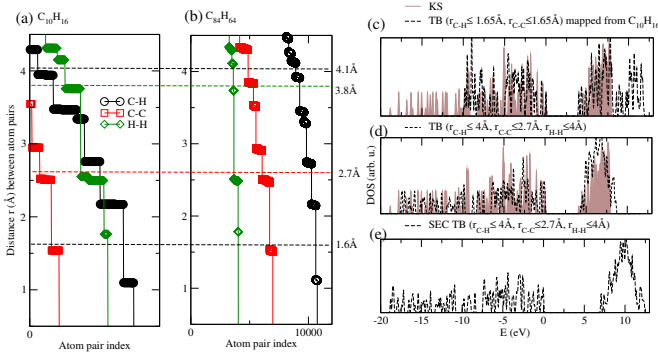


FIG. 15: Distribution of distance between pairs of atoms in (a): reference ($C_{10}H_{16}$) and (b): target ($C_{84}H_{64}$) systems. (c-d): Match between DFT DOS and mapped TB DOS as with an increasing spatial range of neighbourhood considered for mapping. (e): Match between DFT+ G_0W_0 DOS and mapped self-energy corrected TB DOS.

$C_{10}H_{16}$ leading to a good match of not only the SEC-TB mapped band-gap and the QP band-gap calculated at the G_0W_0 level, but also the SE corrected DOS of the valence band[Fig.13(f)].

Next we attempt mapping $C_{26}H_{32}$ from smaller references, starting with mapping from C_3H_8 to $C_{26}H_{32}$, which is about five times increase in system size. Mapping of only nearest neighbour C-C and C-H hopping underestimates band-gap by about 15% [Fig.14(c)]. Mapping all hopping parameters up to upto 4.5Å which is the maximum range of hopping available in the reference, drastically improves overall match of not only mapped TB DOS and DFT DOS [Fig.14(d,e)] but also mapped SEC-TB DOS and DFT+ G_0W_0 DOS [Fig.14(f)], as is seen in case of mapping $C_{10}H_{16}$ from C_3H_8 .

Finally we demonstrate mapping to $C_{84}H_{64}$ from $C_{10}H_{16}$, which is about six time enhancement in system size. Mapping of only the nearest neighbour C-C and C-H bonds results into good match of the mapped TB band-gap [Fig.15(c)] with the DFT band-gap. With further mapping of hopping parameters upto 2.75Å (nn,2n), 4Å (nn,2n+) and 4Å (2n,3n+) [Fig.15(a,b)] for C-C, C-H and H-H pairs, satisfactory match of the entire valence band and a good match [Fig.15(d)] of the band-gap is achieved. Mapping of SEC of TB parameters from $C_{10}H_{16}$ to $C_{84}H_{64}$ results into a QP band-gap of about 7.2 eV which is within 5% deviation from the QP band-gap implied in literature [66–69].

In Fig.16 we show similar mapping of TB parameters at the DFT and DFT+ G_0W_0 levels for Si based nano-diamonds. Like in case of nano-diamonds, mapping of hopping up to second nearest Si neighbours and H atoms associated with them from Si_3H_8 , renders good match of the SEC-TB band-gap with the explicitly estimated DFT+ G_0W_0 band-gap almost up to six times escalation of system size. These results imply consistency in transferability of SEC corrected TB parameters with increasing principal quantum number of valence orbitals.

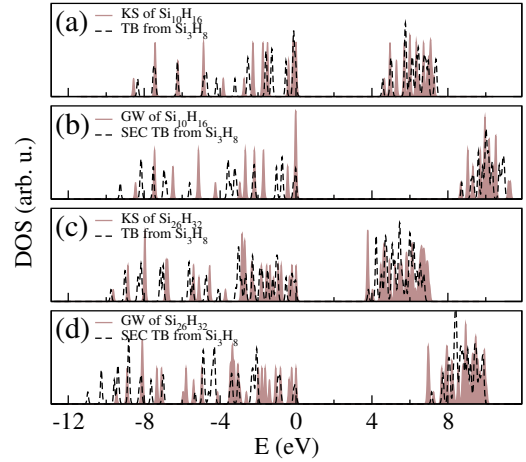


FIG. 16: (a,c): Match between DFT DOS and TB DOS with parameters mapped from Si_3H_8 . (b,d): Match between DFT+ G_0W_0 DOS and SEC-TB DOS using mapped self-energy corrected TB parameters from Si_3H_8 .

III. CONCLUSION

In conclusion, construction of naturalized hybrid atomic orbitals (HAO) is proposed as the common eigenstates of the non-commuting set of finite first-moment matrices corresponding to the orthogonal directions. Hybridization and orientations of HAOs are numerically naturalized as per their anticipated immediate atomic neighbourhood. Choice of gauge based on the HAOs leads to the construction of the hybrid atomic Wannier orbitals (HAWO) from Kohn-Sham (KS) single particle states, rendering a multi-orbital orthonormal tight-binding (TB) basis locked to the nearest neighbourhood. HAWO basis allows calculation of single TB parameters per bond from first principles, and facilitate their easy transfer across iso-structural systems through mapping of immediate atomic neighbourhoods and projection of charge centres learned in the process of naturalization of the HAOs. The mapping allow effective bottom-up transfer of self-energy corrected TB parameters estimated within the GW approximation of many-body perturbation theory in HAWO basis, from smaller reference systems to much larger target systems having similar covalent atomic neighbourhoods, suggesting a possible route towards computationally inexpensive estimation of quasi-particle structures of large covalent systems within acceptable range of accuracy, with extra computational cost scaling as N^2 , beyond the explicit computation of self-energy correction for smaller reference systems which typically scale as N^4 . Demonstrated in nano-ribbons and nano-diamond systems, the transferability of self-energy corrected multi-orbital TB parameters in HAWO basis, is rooted at the spatial localization of the extent of self-energy correction predominantly within the third nearest neighbourhood, which appears to be robust for σ bonds but lesser so with π bonds and unpaired electrons.

IV. ACKNOWLEDGMENTS

Computations have been performed in computing clusters supported by the Nanomission of the Dept. of Sci.&

Tech. and Dept. of Atomic Energy of the Govt. of India.

-
- [1] Linus Pauling. The nature of the chemical bond. application of results obtained from the quantum mechanics and from a theory of paramagnetic susceptibility to the structure of molecules. *Journal of the American Chemical Society*, 53(4):1367–1400, 1931.
- [2] John C Slater. Directed valence in polyatomic molecules. *Physical Review*, 37(5):481, 1931.
- [3] G Doggett. Excited electronic states of diamond. *Proceedings of the Physical Society*, 86(2):393, 1965.
- [4] Giuseppe Del Re. Hybridization and localization in the tight-binding approximation. *Theoretica chimica acta*, 1(2):188–197, 1963.
- [5] Rev McWeeny. Some recent advances in density matrix theory. *Reviews of Modern Physics*, 32(2):335, 1960.
- [6] G Del Re, U Esposito, and M Carpentieri. Bent bonds, hybridization, and the maximum localization criterion. *Theoretica chimica acta*, 6(1):36–44, 1966.
- [7] Alan E Reed, Larry A Curtiss, and Frank Weinhold. Intermolecular interactions from a natural bond orbital, donor-acceptor viewpoint. *Chemical Reviews*, 88(6):899–926, 1988.
- [8] R McWeeny and G Del Re. Criteria for bond orbitals and optimum hybrids. *Theoretica chimica acta*, 10(1):13–22, 1968.
- [9] JN Murrell. Construction of hybrid orbitals. *The Journal of Chemical Physics*, 32(3):767–770, 1960.
- [10] I Mayer. Atomic orbitals from molecular wave functions: The effective minimal basis. *The Journal of Physical Chemistry*, 100(15):6249–6257, 1996.
- [11] I Mayer. Non-orthogonal localized orbitals and orthogonal atomic hybrids derived from mulliken’s population analysis. *Chemical physics letters*, 242(4-5):499–506, 1995.
- [12] a) JP Foster and F Weinhold. Natural hybrid orbitals. *Journal of the American Chemical Society*, 102(24):7211–7218, 1980.
- [13] John C Slater. Atomic shielding constants. *Physical Review*, 36(1):57, 1930.
- [14] Warren J Hehre, Robert F Stewart, and John A Pople. self-consistent molecular-orbital methods. i. use of gaussian expansions of slater-type atomic orbitals. *The Journal of Chemical Physics*, 51(6):2657–2664, 1969.
- [15] Thom H Dunning Jr. Gaussian basis sets for use in correlated molecular calculations. i. the atoms boron through neon and hydrogen. *The Journal of chemical physics*, 90(2):1007–1023, 1989.
- [16] Chang-Guo Zhan and Zhen-Min Hu. Maximum bond order hybrid orbitals. *Theoretica chimica acta*, 84(6):511–520, 1993.
- [17] AB Rives and F Weinhold. Natural hybrid orbitals: Ab initio scf and ci results for co and nico. *International Journal of Quantum Chemistry*, 18(S14):201–209, 1980.
- [18] MS Gopinathan. Determination of atomic hybridization in molecular orbital theory: A valency method. *Journal of Molecular Structure: THEOCHEM*, 169:379–388, 1988.
- [19] Carol A Baxter and David B Cook. Molecular fragments and the hybrid basis. *International journal of quantum chemistry*, 60(1):173–183, 1996.
- [20] EF Kirkwood and DB Cook. Generalized hybrid orbitals. *Theoretica chimica acta*, 44(2):139–149, 1977.
- [21] Jiali Gao, Patricia Amara, Cristobal Alhambra, and Martin J Field. A generalized hybrid orbital (gho) method for the treatment of boundary atoms in combined qm/mm calculations. *The Journal of Physical Chemistry A*, 102(24):4714–4721, 1998.
- [22] Jingzhi Pu, Jiali Gao, and Donald G Truhlar. Generalized hybrid orbital (gho) method for combining ab initio hartree-fock wave functions with molecular mechanics. *The Journal of Physical Chemistry A*, 108(4):632–650, 2004.
- [23] IV Popov, AL Tchougreeff, and R Dronskowski. Deductive molecular mechanics of carbon allotropes. *Low Temperature Physics*, 46(7):655–670, 2020.
- [24] Michael Victor Berry. Quantal phase factors accompanying adiabatic changes. *Proceedings of the Royal Society of London. A. Mathematical and Physical Sciences*, 392(1802):45–57, 1984.
- [25] Raffaele Resta. Macroscopic polarization in crystalline dielectrics: the geometric phase approach. *Reviews of modern physics*, 66(3):899, 1994.
- [26] RD King-Smith and David Vanderbilt. Theory of polarization of crystalline solids. *Physical Review B*, 47(3):1651, 1993.
- [27] Nicola Marzari and David Vanderbilt. Maximally localized generalized wannier functions for composite energy bands. *Physical review B*, 56(20):12847, 1997.
- [28] Joydeep Bhattacharjee and Umesh V Waghmare. Localized orbital description of electronic structures of extended periodic metals, insulators, and confined systems: Density functional theory calculations. *Physical Review B*, 73(12):121102, 2006.
- [29] Jean-François Cardoso and Antoine Souloumiac. Jacobi angles for simultaneous diagonalization. *SIAM journal on matrix analysis and applications*, 17(1):161–164, 1996.
- [30] Herman H Goldstine, Francis J Murray, and John Von Neumann. The jacobi method for real symmetric matrices. *Journal of the ACM (JACM)*, 6(1):59–96, 1959.
- [31] JM Foster and SF Boys. Canonical configurational interaction procedure. *Reviews of Modern Physics*, 32(2):300, 1960.
- [32] Hiroshi Tatewaki and Sigeru Huzinaga. A systematic preparation of new contracted gaussian type orbital set. i. transition metal atoms from sc to zn. *The Journal of Chemical Physics*, 71(11):4339–4348, 1979.
- [33] R Bruce King. Atomic orbitals, symmetry, and coordination polyhedra. *Coordination Chemistry Reviews*, 197(1):141–168, 2000.
- [34] Denis Rafael Nachar, Allan Victor Ribeiro, and Alexys Bruno-Alfonso. A simple geometrical path towards hy-

- brid orbitals. *Materials Research*, 17(6):1474–1476, 2014.
- [35] DM David Jeba Singh, T Pradeep, Joydeep Bhattacharjee, and UV Waghmare. Novel cage clusters of mos2 in the gas phase. *The Journal of Physical Chemistry A*, 109(33):7339–7342, 2005.
- [36] Joydeep Bhattacharjee. Activation of graphenic carbon due to substitutional doping by nitrogen: Mechanistic understanding from first principles. *The journal of physical chemistry letters*, 6(9):1653–1660, 2015.
- [37] Rita Maji and Joydeep Bhattacharjee. Synergistic view of magnetism, chemical activation, and oxygen reduction reaction as well as oxygen evolution reaction catalysis of carbon-doped hexagonal boron nitride from first principles. *The Journal of Physical Chemistry C*, 123(27):16731–16740, 2019.
- [38] Per-Olov Löwdin. On the non-orthogonality problem connected with the use of atomic wave functions in the theory of molecules and crystals. *The Journal of Chemical Physics*, 18(3):365–375, 1950.
- [39] Nicola Marzari, Arash A Mostofi, Jonathan R Yates, Ivo Souza, and David Vanderbilt. Maximally localized wannier functions: Theory and applications. *Reviews of Modern Physics*, 84(4):1419, 2012.
- [40] Young-Su Lee, Marco Buongiorno Nardelli, and Nicola Marzari. Band structure and quantum conductance of nanostructures from maximally localized wannier functions: the case of functionalized carbon nanotubes. *Physical review letters*, 95(7):076804, 2005.
- [41] Dominik Gresch, QuanSheng Wu, Georg W Winkler, Rico Häuselmann, Matthias Troyer, and Alexey A Soluyanov. Automated construction of symmetrized wannier-like tight-binding models from ab initio calculations. *Physical Review Materials*, 2(10):103805, 2018.
- [42] Arrigo Calzolari, Nicola Marzari, Ivo Souza, and Marco Buongiorno Nardelli. Ab initio transport properties of nanostructures from maximally localized wannier functions. *Physical Review B*, 69(3):035108, 2004.
- [43] CESARE Franchini, R Kováčik, Martijn Marsman, S Sathyanarayana Murthy, Jiangang He, Claude Ederer, and Georg Kresse. Maximally localized wannier functions in lamno3 within pbe+ u, hybrid functionals and partially self-consistent gw: an efficient route to construct ab initio tight-binding parameters for eg perovskites. *Journal of Physics: Condensed Matter*, 24(23):235602, 2012.
- [44] Jeil Jung and Allan H MacDonald. Tight-binding model for graphene π -bands from maximally localized wannier functions. *Physical Review B*, 87(19):195450, 2013.
- [45] Xiaofeng Qian, Ju Li, Liang Qi, Cai-Zhuang Wang, Tzu-Liang Chan, Yong-Xin Yao, Kai-Ming Ho, and Sidney Yip. Quasiatomic orbitals for ab initio tight-binding analysis. *Physical Review B*, 78(24):245112, 2008.
- [46] Xiaofeng Qian, Ju Li, and Sidney Yip. Calculating phase-coherent quantum transport in nanoelectronics with ab initio quasiatomic orbital basis set. *Physical Review B*, 82(19):195442, 2010.
- [47] Pino D’Amico, Luis Agapito, Alessandra Catellani, Alice Ruini, Stefano Curtarolo, Marco Fornari, Marco Buongiorno Nardelli, and Arrigo Calzolari. Accurate ab initio tight-binding hamiltonians: effective tools for electronic transport and optical spectroscopy from first principles. *Physical Review B*, 94(16):165166, 2016.
- [48] Luis A Agapito, Marco Fornari, Davide Ceresoli, Andrea Ferretti, Stefano Curtarolo, and Marco Buongiorno Nardelli. Accurate tight-binding hamiltonians for two-dimensional and layered materials. *Physical Review B*, 93(12):125137, 2016.
- [49] Sheng-Ying Yue, Guangzhao Qin, Xiaoliang Zhang, Xianlei Sheng, Gang Su, and Ming Hu. Thermal transport in novel carbon allotropes with s p 2 or s p 3 hybridization: An ab initio study. *Physical Review B*, 95(8):085207, 2017.
- [50] Ilya V Popov, Victor V Slavin, Andrei L Tchougréeff, and Richard Dronskowski. Deductive molecular mechanics of four-coordinated carbon allotropes. *Physical Chemistry Chemical Physics*, 21(33):18138–18148, 2019.
- [51] Kenneth B Wiberg. Bent bonds in organic compounds. *Accounts of chemical research*, 29(5):229–234, 1996.
- [52] Lars Hedin. New method for calculating the one-particle green’s function with application to the electron-gas problem. *Physical Review*, 139(3A):A796, 1965.
- [53] Lars Hedin and Stig Lundqvist. Effects of electron-electron and electron-phonon interactions on the one-electron states of solids. In *Solid state physics*, volume 23, pages 1–181. Elsevier, 1970.
- [54] Mark S Hybertsen and Steven G Louie. Electron correlation in semiconductors and insulators: Band gaps and quasiparticle energies. *Physical Review B*, 34(8):5390, 1986.
- [55] Alexander N Rudenko and Mikhail I Katsnelson. Quasiparticle band structure and tight-binding model for single-and bilayer black phosphorus. *Physical Review B*, 89(20):201408, 2014.
- [56] Irene Aguilera, Christoph Friedrich, and Stefan Blügel. Many-body corrected tight-binding hamiltonians for an accurate quasiparticle description of topological insulators of the bi 2 se 3 family. *Physical Review B*, 100(15):155147, 2019.
- [57] Jin Yu, Mikhail I Katsnelson, and Shengjun Yuan. Tunable electronic and magneto-optical properties of monolayer arsenene: From gw 0 approximation to large-scale tight-binding propagation simulations. *Physical Review B*, 98(11):115117, 2018.
- [58] Alexander Grüneis, Claudio Attaccalite, Ludger Wirtz, H Shiozawa, R Saito, Thomas Pichler, and Angel Rubio. Tight-binding description of the quasiparticle dispersion of graphite and few-layer graphene. *Physical Review B*, 78(20):205425, 2008.
- [59] Yeongsu Cho and Timothy C Berkelbach. Optical properties of layered hybrid organic–inorganic halide perovskites: A tight-binding gw-bse study. *The Journal of Physical Chemistry Letters*, 10(20):6189–6196, 2019.
- [60] Akitaka Sawamura, Jun Otsuka, Takashi Kato, and Takao Kotani. Nearest-neighbor sp3s* tight-binding parameters based on the hybrid quasi-particle self-consistent gw method verified by modeling of type-ii superlattices. *Journal of Applied Physics*, 121(23):235704, 2017.
- [61] Paolo Giannozzi, Stefano Baroni, Nicola Bonini, Matteo Calandra, Roberto Car, Carlo Cavazzoni, Davide Ceresoli, Guido L Chiarotti, Matteo Cococcioni, Ismaila Dabo, et al. Quantum espresso: a modular and open-source software project for quantum simulations of materials. *Journal of physics: Condensed matter*, 21(39):395502, 2009.
- [62] John P Perdew and Alex Zunger. Self-interaction correction to density-functional approximations for many-electron systems. *Physical Review B*, 23(10):5048, 1981.
- [63] Jack Deslippe, Georgy Samsonidze, David A Strubbe,

- Manish Jain, Marvin L Cohen, and Steven G Louie. Berkeleygw: A massively parallel computer package for the calculation of the quasiparticle and optical properties of materials and nanostructures. *Computer Physics Communications*, 183(6):1269–1289, 2012.
- [64] Li Yang, Cheol-Hwan Park, Young-Woo Son, Marvin L Cohen, and Steven G Louie. Quasiparticle energies and band gaps in graphene nanoribbons. *Physical Review Letters*, 99(18):186801, 2007.
- [65] Manoar Hossain and Joydeep Bhattacharjee. Transferability of self-energy correction in tight-binding basis constructed from first principles. *The Journal of Chemical Physics*, 153(14):144103, 2020.
- [66] Jean-Yves Raty and G Galli. Optical properties and structure of nanodiamonds. *Journal of Electroanalytical Chemistry*, 584(1):9–12, 2005.
- [67] Jean-Yves Raty, Giulia Galli, C Bostedt, Tony W Van Buuren, and Louis J Terminello. Quantum confinement and fullerene-like surface reconstructions in nanodiamonds. *Physical review letters*, 90(3):037401, 2003.
- [68] ND Drummond, AJ Williamson, RJ Needs, and G Galli. Electron emission from diamondoids: a diffusion quantum monte carlo study. *Physical review letters*, 95(9):096801, 2005.
- [69] Takao Sasagawa and Zhi-xun Shen. A route to tunable direct band-gap diamond devices: Electronic structures of nanodiamond crystals. *Journal of applied physics*, 104(7):073704, 2008.